XAFS determination of the bacterial cell wall functional groups responsible for complexation of Cd and U as a function of pH

S. D. Kelly,[a] M. I. Boyanov,[b] B. A. Bunker,[b] J. B. Fein,[b] D. A. Fowle,[b,c] N. Yee[b] and K. M. Kemner[a]

[a]Argonne National Laboratory, Argonne, IL, 60439, USA, [b]University of Notre Dame, Notre Dame, IN, 46556, USA, and [c]present address: University of Windsor, Windsor, ON N9B 3P4, Canada

Bacteria, which are ubiquitous in near-surface geologic systems, can affect the distribution and fate of metals in these systems through adsorption reactions between the metals and bacterial cell walls. Recently, Fein *et al.* (1997) developed a chemical equilibrium approach to quantify metal adsorption onto cell walls, treating the sorption as a surface complexation phenomenon. However, such models are based on circumstantial bulk adsorption evidence only, and the nature and mechanism of metal binding to cell walls for each metal system have not been determined spectroscopically. The results of XAFS measurements at the Cd K-edge and U L3-edge on *Bacillus subtilis* exposed to these elements show that, at low pH, U binds to phosphoryl groups while Cd binds to carboxyl functional groups.

Keywords: Environmental science; **biogeochemistry**; **microbiology**; **uranium**; **cadmium.**

1. Introduction

Bacteria, which are ubiquitous in near-surface geologic systems, can affect the distribution and fate of metals in these systems through adsorption reactions between the metals and bacterial cell walls. Many studies have addressed relative binding capacities of metals to cell walls (Ribbe, 1997). Recently, Fein *et al.* (1997) developed a chemical equilibrium approach to quantify metal adsorption onto Gram positive cell walls, treating the sorption as a surface complexation phenomenon. The authors used acid/base titrations to determine acidity constants for the important surface functional groups, and they used metal adsorption experiments to yield site-specific stability constants for the metal-bacteria surface complexes. This approach implies that different functional group types have different pH ranges in which they deprotonate and adsorb metals from solution. Fein *et al.* (1997) observed negligible Cd adsorption under low-pH conditions, with adsorption increasing with increasing pH above approximately pH 3.0 as the surface functional groups sucessively deprotonated. Fowle *et al.* (2000) observed a similar pH dependence for UO_2^{+2} adsorption onto the same bacteria, but they also observed significant uranyl adsorption even under low-pH conditions. Fowle *et al.* (2000) ascribed the low-pH adsorption to an interaction between the uranyl cation and a neutrally charged phosphoryl group on the cell wall. However, all of these models are based on circumstantial bulk adsorption evidence only, and the nature and mechanism of metal binding to the cell walls for each metal system has not been determined. X-ray absorption fine structure (XAFS) measurements at the complexed metal absorption edge can distinguish between the different functional groups proposed to be important in metal uptake, thereby proving or disproving the proposed surface complexation models.

2. Methods

Samples of Cd and U adsorbed to cultures of *B. subtilis* were prepared by exposing aqueous Cd and U solutions to a known concentration of biomass, so that the ratio of metal to cell surface area remained constant. To probe pH-dependent changes in the adsorption mechanism, samples were prepared as a function of pH, from pH 1 to 5 for the U biomass samples and from pH 2.5 to 10 for the Cd biomass samples. Only the lowest-pH samples are discussed here. Sample preparation details are described elsewhere (Fowle & Fein, 2000). The biomass solution was centrifuged, and fluorescence XAFS measurements were made on the wet homogeneous paste. All XAFS measurements were made at the Materials Research Collaborative Access Team (MR-CAT) sector 10-ID beamline at the Advanced Photon Source (Segre *et al.*, 2000).

The beamline optics and setup parameters for the Cd K-edge measurements were as follows: The Si(333) reflection of the double-crystal monochromator running on the fifth harmonic of the beamline undulator was used. The fundamental energy was blocked with a 3-mm-thick, 30-adsorption-lengths aluminum plate. Higher harmonics were rejected by using a Pt mirror at approximately 1.9 mrad relative to the incident beam direction. The fluorescence data were taken by using a fluorescence detector filled with Kr gas. The incident and transmitted x-ray ion chambers were filled with nitrogen and a 1:1 mixture of nitrogen:argon gas, respectively.

For the U L3-edge measurements, the Si(111) reflection of the double-crystal monochromator running on the third harmonic of the beamline undulator was used. Higher harmonics were rejected by using a Rh mirror. The fluorescence detector was filled with argon gas, and the incident and transmitted ion chambers were both filled with nitrogen gas.

For both the U and Cd measurements, the undulator was tapered approximately 2 keV to reduce the variation in the incident intensity to about 15% over the scanned energy range. Linearity tests (Kemner *et al.*, 1994) indicated less than 0.3% nonlinearity for a 50% decrease in incident intensity. To minimize radiation exposure, the X-ray beam was reduced to 0.7 mm square, and the data were collected by using slew scanning mode. Data were collected at six sample locations, with 2 to 5 scans at each. Slew scanning mode allows data collection in the X-ray absorption near edge structure (XANES) region or extended X-ray absoprtion fine structure (EXAFS) region in approximately one minute. Measuring several spectra at each location allows for the determination of radiation-induced chemical effects at the one-minute time scale. No change in the XANES or EXAFS spectra was found for any of the samples.

The theoretical $\chi(k)$ was constructed by using the program FEFF7 (Zabinsky *et al.*, 1995). The data were analyzed with codes from the UWXAFS package (Stern *et al.*, 1995). The error analysis and the goodness-of-fit parameters were calculated by the fitting routine FEFFIT (Newville, 1994). Listed with the fit results are the XAFS reliability factor $\mathcal{R}$ and the reduced-chi-squared value χ^2_ν (Newville, 1994). Quoted errors in the fitted variables include systematic contributions introduced from measurement, theory, and analysis (Stern *et al.*, 1995).

The U L3 XAFS measurements were taken in fluorescence and transmission modes. Two EXAFS measurements were taken at

three different spots for a total of six measurements. The background was removed by using the AUTOBK program (Newville *et al*, 1993). The resulting six chi data sets were averaged. The average $\chi(k)$ data is shown in Fig. 1a.

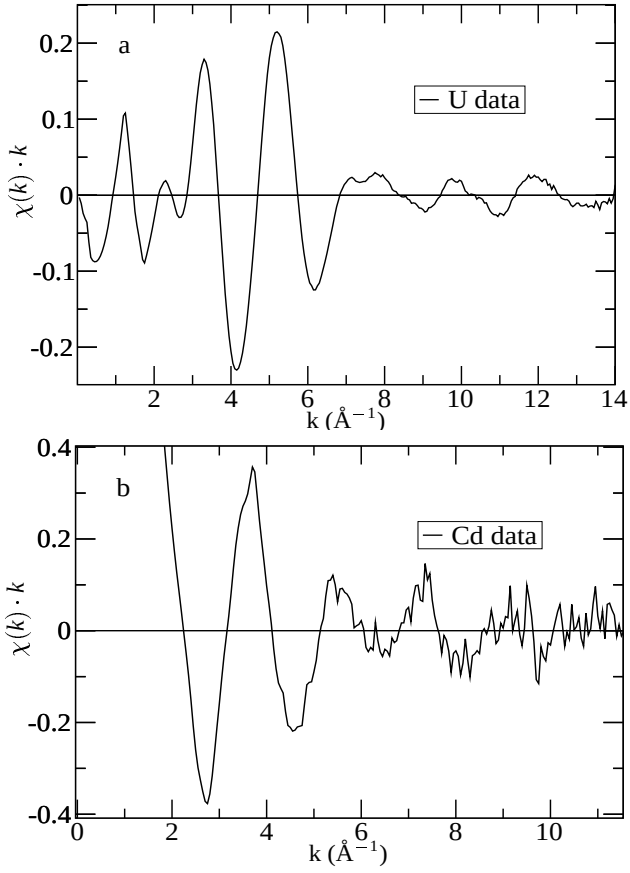

Figure 1
Average $\chi(k)\cdot k$ data for the biomass samples (a) U data at pH 1.67 (b) Cd data at pH 3.5.

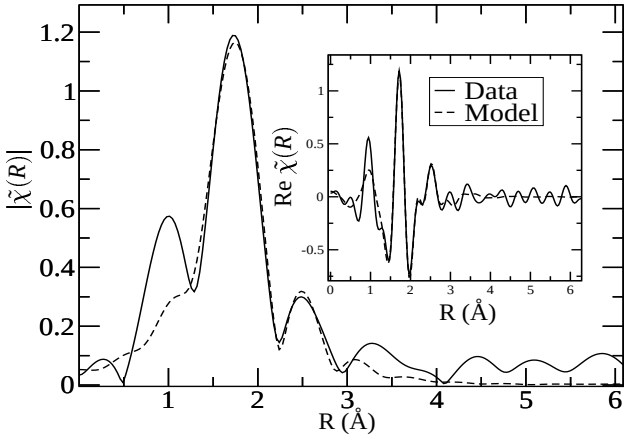

Figure 2
The magnitude, $|\tilde{\chi}(R)|$, and real part, Re $\tilde{\chi}(R)$ (inset), of the Fourier transform of the $\chi(k)\cdot k$ best-fit model and data from the Cd-biomass sample at pH 3.5. The data range $\Delta k = [3 : 9.25]$Å^{-1} was used in the Fourier transform.

Five successive Cd EXAFS fluorescence measurements were made at 5 different locations on the biomass samples, for a total of 25 measurements. The 5 μ(E)·x data sets taken at each spot were averaged before the background was removed. The 5 resulting $\chi(k)$ data sets were averaged. The average $\chi(k)$ is shown in Fig. 1b. The relative concentration of U absorbed to the biomass was aproximately 50 times greater than that of Cd; therefore the U signal was much cleaner, and fewer averaged data sets were required.

Several Cd-acetate solutions with different concentrations of Cd were also measured in fluorescence and transmission modes. Comparison of the XAFS fluorescence and transmitted signals showed that a Cd concentration of 80 mM resulted in a 17% reduction in the fluorescence signal. The amount of Cd in each biomass sample was estimated by comparing the step height of the fluorescence signal from the biomass to that of the solution standards. To determine the fluorescence corrections (Pfalzer *et al.*, 1999), the transmission $\chi(k)$ value was divided by the fluorescence $\chi(k)$ value for each concentration of the Cd-acetate solution.

An initial step in the analysis is determination of the value for S_0^2, the passive electron amplitude reduction factor. Both S_0^2 and σ_i^2 affect the XAFS amplitude and are highly correlated. Because of the different k dependencies of these terms, multiple k-weighted fitting of the data was used to break their correlation (Kelly *et al.*, to be published).

Table 1
Best-fit values for the Cd-biomass data at pH 3.5, with goodness-of-fit parameters. The subscript c indicates that the parameter was determined in the fit but was constrained as explained in the text. The model names P, C, and H stand for physphoryl, carboxyl, and hydroxyl, respectively. The χ^2_ν values for the models are 13, 11, and 12, respectively.

Model	Path	N_{degen}	R (Å)	σ^2 (10^{-3}Å^2)	$\mathcal{R}$
P	Cd→O	6.1±1.1	2.27±0.01	6±2	0.032
	Cd→P	1.0±1.0	3.34±0.08	6_c	
C	Cd→O	5.8±1.0	2.28±0.01	5±2	0.028
	Cd→C	3.0±1.6	3.13±0.06	5_c	
H	Cd→O	6.8±1.1	2.28±0.02	7±2	0.047

3. Results and Discussion

For both the Cd and U data, three models were needed to describe binding to hydroxyl, phosphoryl, and carboxyl functional groups. Theoretical models for cadmium acetate dihydrate (Harisson & Trotter, 1972), cadmium phosphate (Bigi *et al.*, 1986), sodium uranyl triacetate (Templeton *et al.*, 1985), hydrogen uranyl phosphate tetrahydrate (Morosin, 1978) were generated by FEFF7. The difference in data due to the different binding models will be in the second shell, were we expect to find a signal from a P, C, or H for the phosphoryl, carboxyl, or hydroxyl functional group. For the hydroxyl binding mechanism, the signal is expected to be similar to that for hydrated U/Cd. The U/Cd hydroxide was simulated by taking the paths from the first oxygen shell surrounding the U/Cd in previous structures. Several solution standards of hydrated U/Cd, U/Cd-acetate, and U/Cd-phosphate were measured to simulate the hydroxyl, carboxyl, and phosphoryl binding in the biomass samples.

For the Cd-acetate and Cd-phosphate solution standards, a two-shell (O and then P/C) fit was sufficient to distinguish acetate from phosphate. In these models, σ^2 was constrained for both shells (O and P/C) to the same value. This constraint reduced the χ^2_ν significantly (by a factor of 30). Both the Cd-acetate and Cd-phosphate

models, along with a single O shell model (to represent a Cd-hydroxyl) were applied to the Cd-biomass data at pH 3.5. The results are in Table 1. The Cd-phosphate model gives a degeneracy of the P shell that is consistent with zero, indicating that the P shell is not significantly improving the fit quality. The larger $\mathcal{R}$ value of 0.047 (Newville, 1994) for the Cd-hydroxyl model indicates that it is not optimal for the data. The Cd-acetate model gives the best fit with reasonable fit parameters. The data and the best-fit model are shown in Fig. 2.

First a model for a hydrated uranyl standard was developed, and the values were used as input parameters in FEFF7 to create a theoretical fit for a hydrated uranyl. This model was then used to generate a fit to the experimental data for the U-biomass sample. The best-fit values for the fits to the U-biomass sample and the hydrated uranyl sample are similar, giving confidence in this model for the biomass sample. However, careful consideration of the data between 2.5 and 3.8 Å indicates the presence of an additional atom(s) surrounding the U atoms in the biomass sample.

Table 2

Models considered for the data in the region at 2.5-4.0 Å in the U-biomass $|\tilde{\chi}(R)|$ data, listed in order of increasing χ^2_ν. S.S. and M.S. stand for single- and multiple-scattering paths, respectively. Initial path lengths of 2.6 and 2.9 Å were used for the short and long paths, respectively.

Model Name	Path description	$\mathcal{R}$	χ^2_ν	ν
fit-mPP	M.S. O-P and S.S long P	0.08	13	7
fit-PP	S.S. short P and long P	0.05	16	6
fit-PO	S.S. short P and long O	0.13	28	6
fit-mPC	M.S. O-P and S.S long C	0.11	32	6
fit-OP	S.S. short O and long P	0.19	36	6
fit-mP	M.S. O-P	0.20	46	9
fit-P2	S.S. long P	0.22	50	9
fit-P1	S.S. short P	0.31	82	9
fit-CC	S.S. short C and long C	0.29	100	5

Table 3

Best-fit values for the U-biomass samples at pH 1.67. These fits had 22.6 independent points in the data and 15 variables. $E_0 = 4.4 \pm 1.1$.

Path	N_{degen}	R (Å)	σ^2 (10^{-3}Å^2)
U→Oax	2.0	1.777 ± 0.006	1.2 ± 0.3
U→Oeq	6.3 ± 0.5	2.387 ± 0.009	9.1 ± 1.3
U→Oax1→U→Oax1	2.0	3.553 ± 0.011	2.5 ± 0.7
U→Oax1→Oax2→U	2.0	3.553 ± 0.011	2.5 ± 0.7
U→Oax1→U→Oax2→U	2.0	3.553 ± 0.011	2.5 ± 0.7
U→P1	1.0 ± 0.8	3.628 ± 0.038	5.7 ± 5.0
U→P2	1.9 ± 1.3	3.904 ± 0.027	5.7 ± 5.0

With the hydrated uranyl model held constant, this region (2.5 to 3.8 Å) was modeled with several different combinations of single- and multiple-scattering C, O, and, P shells. The different models and the goodness-of-fit values for these models are in Table 2. Two statistically equivalent best-fit models are at the top of Table 2. One consists of two single-scattering U→P paths, and the other consists of all the multiple-scattering U→Oeq→P paths and a single-scattering U→P path. Both models are consistent with two phosphate binding sites. Finally, the U-biomass data were fitted over the entire R-space range (1 to 3.8 Å) by using the paths from the hydrated uranyl model and the two single-scattering U→P paths. The best-fit values to these data are in Table 3. The quality of the fit to the data is illustrated in Fig. 3.

In summary, XAFS can be used to distinguish hydroxyl, carboxyl, and phosphoryl bonding to metals in biomass. These preliminary results at the lowest pH are consistent with the surface complexation models proposed by Fein *et al.* (1997) and Fowle *et al.* (2000). We plan to use this technique to investigate pH-dependent sorption to cell walls.

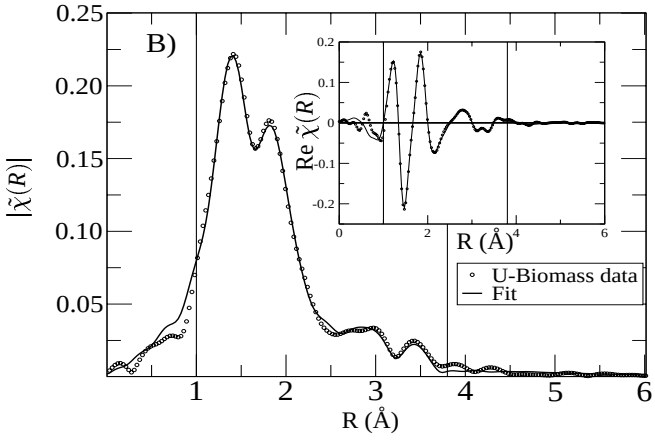

Figure 3

The magnitude, $|\tilde{\chi}(R)|$, and real part, Re $\tilde{\chi}(R)$ (inset), of the Fourier transform of the $\chi(k)\cdot k$ best-fit model, with data from the U-biomass sample at pH 1.67. The data range $\Delta k = [2.5 : 13.5]$ Å^{-1} was used in the Fourier transform.

Support for SDK and KMK was provided by the U.S. Department of Energy (DOE), Office of Science, Office of Biological and Environmental Research, NABIR Program, and use of the MR-CAT sector of the APS was supported by the DOE Office of Basic Energy Sciences, both under contract W-31-109-Eng-38. Other support was provided by National Science Foundation grant EAR-9905704 and by the donors of the Petroleum Research Fund, administered by the American Chemical Society.

References

Bigi, A., Foresti, E., Gazzano, M., Ripamonti, A. & Roveri, N. (1986). *J. Chem. Research*, **35**, 170.

Fein, J. B., Daughney, C. J., Yee, N. & Davis, T. A. (1997). *Geochim. Cosmochim. Acta*, **61**(16), 3319.

Fowle, D. A. & Fein, J. B. (2000). *Chemical Geology*, **168**, 27–36.

Fowle, D. A., Fein, J. B. & Martin, A. M. (2000). *Environ. Sci. Technol.*, **34**(17), 3737–3741.

Harrison, W. & Trotter, J. (1972). *Chem. Soc. Dalton Trans.* 956.

Kelly, S. D., Ingalls, R. & Stern, E. A. (to be published). *Phys. Rev. B*.

Kemner, K. M., Kropf, J. & Bunker, B. A. (1994). *Rev. Sci. Instrum.*, **65**, 3667–3669.

Morosin, B. (1978). *Acta Crystallography*, B**34**, 3732–3834.

Newville, M., (1994). FEFFIT: Using FEFF to model XAFS in *R*-space. unpublished. This documentation is part of the UWXAFS3.0 package.

Newville, M., Līviņš, P., Yacoby, Y., Rehr, J. J. & Stern, E. A. (1993). *Phys. Rev. B*, **47**(21), 14126–14131.

Pfalzer, P., Urbach, J. P., Klemm, M., & Horn, S. (1999). *Phys. Rev. B*, **60**(13), 9335.

Ribbe, P. (ed.) (1997). *Geomicrobiology: Interactions between Microbes and Minerals*, vol. 35 of *Reviews in Mineralogy*, chap. 5. Washington, D.C.: Mineralogical Society of America.

Segre, C. U., Leyarovska, N. E., Chapman, L. D., Lavender, W. M., Plag, P. W., King, A. S., Kropf, A. J., Bunker, B. A., Kemner, K. M., Dutta, P., Duran, R. S. & Kaduk, J. (2000). In *Synchrotron Radiation Instrumentation: Eleventh U.S. National Conference*, edited by P. Pianetta, *et al.*, vol. CP521, pp. 419–422. New York: American Insitute of Physics.

Stern, E. A., Newville, M., Ravel, B., Yacoby, Y. & Haskel, D. (1995). *Physica B*, **208&209**, 117–120.

Templeton, D., Zalkin, A., Ruben, H., & Templeton, L. (1985). *Acta Crystallography*, C**41**, 1439–1441.

Zabinsky, S. I., Rehr, J. J., Ankudinov, A., Albers, R. C. & Eller, M. J. (1995). *Phys. Rev. B*, **52**(4), 2995–3009.